Lucien M. Levy, MD, PhD • Giovanni Di Chiro, MD • Rodney A. Brooks, PhD • Andrew J. Dwyer, MD • Louis Wener, MD • Joseph Frank, MD

# Spinal Cord Artifacts from Truncation Errors during MR Imaging[1]

**The significance of linear regions of altered signal intensity that appear in sagittal magnetic resonance (MR) images along the length of the spinal cord was investigated. Examinations were performed on ten healthy volunteers and one patient with spinal cord edema. A 0.5-T or a 1.5-T MR system was used. Sampling-related effects (Gibbs phenomenon) at spinal cord edges and cerebrospinal fluid interfaces can lead to different signal patterns within the spinal cord and canal. These artifacts cause problems in interpretation, especially with the use of small object-to-pixel size ratios, by obscuring anatomy and simulating pathologic conditions such as pseudosyringes. Analysis of these intensity variations and of their dependence on sampling may improve the clinical accuracy of MR imaging.**

**Index terms:** Magnetic resonance (MR), artifact • Spinal cord, diseases, 31.365 • Spinal cord, MR studies, 30.1214

**Radiology 1988;** 166:479–483

THE two-dimensional Fourier transform (2DFT) technique in magnetic resonance (MR) imaging has been associated with various artifacts (1–7). Knowledge of their appearances and behaviors is essential for accurate evaluation of normal anatomy and disease. In a number of sagittal MR images of the spine, we observed artifacts that appeared as linear regions of low intensity along the length of the spinal cord. These artifacts could be interpreted as arising from central gray matter (8) and may mimic pathologic conditions such as a dilated central canal, a syrinx, an arteriovenous malformation, or longitudinal necrosis. To assess the role of image resolution (9, 10) and boundary effects (2) in the generation of these lines, we examined ten healthy volunteers and one patient with proved spinal cord disease with various imaging and sampling conditions.

## SUBJECTS AND METHODS

Studies were performed with a 0.5-T superconducting system (Picker International, Highland Heights, Ohio) or a 1.5-T superconducting system (Signa; General Electric Medical Systems Group, Milwaukee). Ten healthy volunteers and one patient with spinal cord edema due to increased venous pressure were examined. Multisection imaging was performed in the sagittal plane with conventional T1- and T2-weighted spin-echo (SE) pulse sequences. The sequences used were repetition time (TR) 500 msec and echo times (TE) of 26 and 30 msec (SE 500/26 and 500/30) and SE 2,000/80 and 2,000/100. In three cases, the T2-weighted images were acquired with a motion artifact suppression technique (MAST) (11, 12). Sections were contiguous and 3 or 5 mm thick. For the healthy volunteers, cardiac-gated images were also obtained with multiecho pulsing sequences and TEs of 30, 60, and 90 msec. All acquisitions were gated to the peak of the R wave of the electrocardiogram (ECG) and obtained at 100-msec intervals throughout the cardiac cycle; TR ranged from 1,000 to 2,000 msec, depending on the subject's heart rate. The sampling frequency along the phase coordinate was determined with the number of phase-encoding gradient steps, and the sampling frequency in the frequency coordinate was determined with the digital sampling rate of the analog signal observed during the readout interval. The phase and frequency data were then used to reconstruct an MR image with the 2DFT technique. The data sampling frequencies varied from 128 to 256 in the phase-encoding direction and from 256 to 512 in the frequency-encoding direction. In seven cases, phase and frequency axes were interchanged. The field of view (FOV) ranged from 16 to 30 cm, and one to four excitations were used for each acquisition.

The effect of flow on the appearance of truncation artifacts was investigated with a simple flow phantom. Plastic tubing with a 0.8-cm inner diameter and a total length of 50 feet (15 m) was used and connected to a large gravity feed tank containing water. The flow rate was adjusted with a valve at the efflux line. The net flow velocities were obtained by measuring inflow with a graduated cylinder and were 0, 0.5, 2.0, 2.8, 4.0, and 6.0 cm/sec, which covered the physiologic range of cerebrospinal fluid (CSF) flow (13). The input line had a course of 2 m within the bore of the magnet to ensure essentially complete magnetization of water. A U-shaped part of the tubing was positioned in a 12 × 18-cm basin that was filled with water to a depth of 8 cm. Sections parallel to the direction of flow and through the tubing were obtained with SE 700/26. The readout gradient direction was parallel to the flow axis. The image consisted of 128 and 512 steps in the phase- and frequency-encoding directions, respectively, with an FOV of 25 cm and a section thickness of 5 mm.

## RESULTS

The effects of sampling and other factors such as pulsing sequence, flow, and pathologic conditions on the patterns of signal intensity across the spinal cord were evaluated. In all healthy volunteers, midline sagittal,

[1] From the Neuroimaging Section, National Institute of Neurological and Communicative Disorders and Stroke (L.M.L., G.D.C., R.A.B.) and the Diagnostic Radiology Department (A.J.D., J.F.), Bethesda, Md.; and Magnetic Resonance Imaging Associates, Clinton, Md. (L.W.). Received June 9, 1987; revision requested July 28; revision received September 8; accepted September 10. **Address reprint requests to** G.D.C., Neuroimaging Section, Building 10, Room 1C451, National Institutes of Health, Bethesda, MD 20892.



See also the article by Bronskill et al. (pp. 485–488) in this issue.

T1-weighted images of the cervical spine showed a dark line located centrally along the length of the spinal cord (Fig. 1a). This pattern was observed when the pixel size was approximately one-fourth of the spinal cord diameter, such as would occur with a pixel width of 2 mm compared with a sagittal spinal cord diameter of about 8 mm.

The artifactual central line may be produced with an FOV of 25 cm and 128 samples in the horizontal direction. When the pixel size was reduced by decreasing the FOV, the single central line was replaced by two or more equally spaced parallel lines along the length of the spinal cord (Fig. 1b). On a long TR multiecho sequence, a cardiac-gated SE image obtained from a healthy volunteer with a 200-msec delay after the R wave of the ECG showed that the CSF became isointense when compared with the intensity of the spinal cord on the second echo (even-echo rephasing) with a resultant loss of contrast at the edges of the spinal cord (Fig. 2). Instead of a single central line, two or more parallel dark lines appeared along the length of the spinal canal (Fig. 2b, 2c).

A patient with a cranial arteriovenous malformation and cervical spinal cord edema (related to increased venous pressure) was thought to have a possible syrinx (Fig. 3a). This cavity, which appeared more prominently than those of healthy volunteers, disappeared when horizontal sampling was increased (Fig. 3b).

In seven cases, phase- and frequency-encoding gradient directions were switched with 128 and 512 steps in each direction, respectively. When horizontal sampling was increased, the dark central band disappeared and the vertical parallel bands overlying the vertebral bodies became horizontal while retaining their spacing in all seven cases (Fig. 4).

The phantom flow studies provided supportive experimental correlation with the spinal images. With the water stationary, a dark line was seen centrally along the length of the plastic tubing (Fig. 5a). Equidistant bands parallel to the edges of the tubing were also seen; they became progressively less prominent at greater distances from the boundaries. As the velocity was increased, the intraluminal signal progressively decreased, especially peripherally. The parallel bands on either side of the tubing remained present, however (Fig. 5b–5d). No new bands were seen.

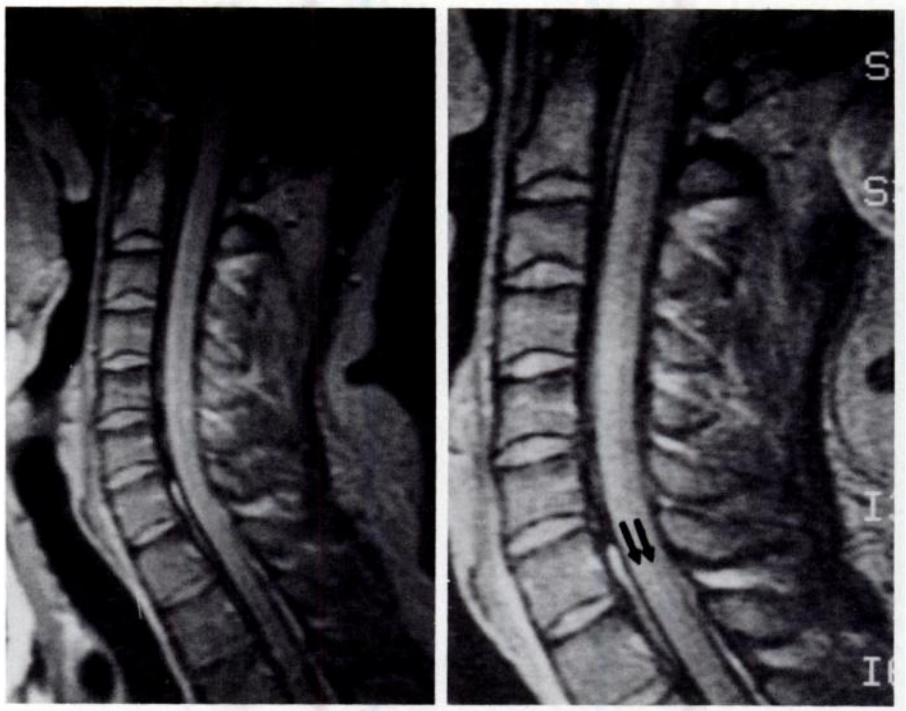


a. b.

**Figure 1.** Sagittal cervical spine images from a healthy volunteer obtained at different sampling rates with cardiac gating, delay of 200 msec, SE 1,000/25, and section thickness of 3 mm. **(a)** Phase- (horizontal) and frequency- (vertical) encoding directions contain 128 × 256 steps; FOV is 24 cm. A dark central band is seen in the spinal cord. Pixel size is one-fourth the spinal cord diameter. **(b)** Phase- and frequency-encoding directions contain 128 × 256 steps; FOV is 16 cm. Note the parallel dark bands (arrows) located centrally in the spinal cord. Pixel size is one-sixth the spinal cord diameter.

## DISCUSSION

In most MR systems, a 2DFT technique is used to reconstruct spatial intensity data from phase- and frequency-encoded information. The image intensity data are obtained with a Fourier series, which is a summation of sinusoidal waves of different amplitudes, phases, and frequencies (14, 15). Sharp edges or discontinuities are difficult to represent since they would ideally require an infinite number of terms (frequencies) in the series. In MR imaging, by virtue of the time constraints placed on data acquisition and image reconstruction, the number of terms is limited by the elimination or truncation of the higher-order terms, which leads to aliasing errors in the reconstruction of the desired object (14–16). Actually, a discrete version of the Fourier transform is used for image reconstruction, which bears close resemblance to the continuous 2DFT and is also affected by truncation errors (14). At abrupt transitions in signal magnitude, loss of the higher-frequency terms results in a variable overshoot and undershoot oscillation, which accentuates high-contrast boundaries (Fig. 6). This is called the Gibbs phenomenon (14, 15). It occurs on both sides of the discontinuity and is associated with a reduction in edge sharpness (slope of spatial intensity profile) and secondary ripples that decay rapidly in a direction perpendicular to the boundary. Decreasing the pixel size by increasing the number of samples at a given FOV decreases both the wavelength and the amplitude of the secondary ripples. In our situation, the wavelength of the ripples is equivalent to the length of two pixels (10). However, the degree of overshoot at the edge amounts to approximately 9% of the discontinuity amplitude, regardless of the number of terms in the series (14).

Although the occurrence of the Gibbs phenomenon is predictable near high-contrast anatomic boundaries, its presence can obscure normal anatomy or pathologic conditions and may simulate disease. It may also be confused with other boundary artifacts (2), flow phenomena, linear foci of calcification, or even paramagnetic effects. The differential features of other edge effects have been reported (2, 3). Chemical shift produces spatial misregistration at interfaces between well-hydrated structures

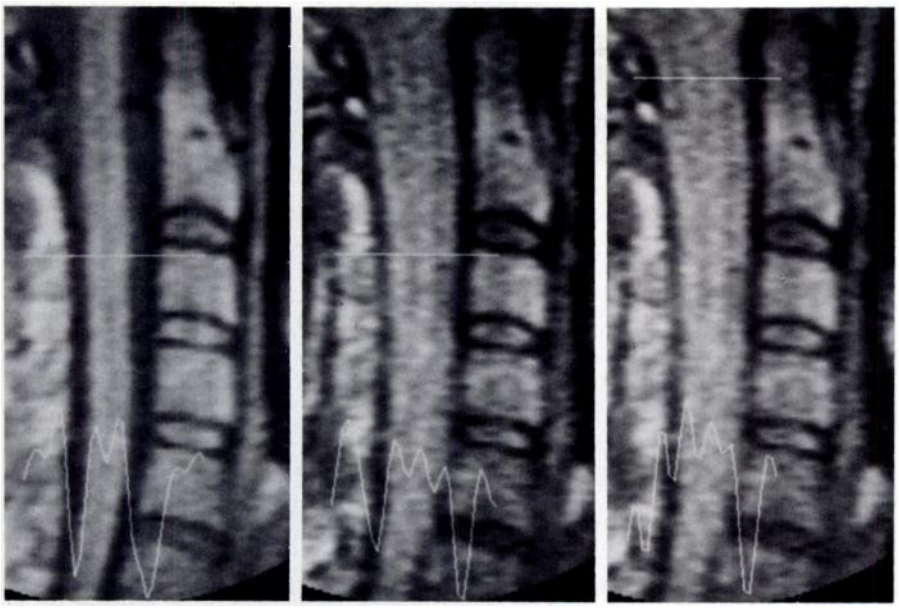

a. b. c.

**Figure 2.** Sagittal cervical spine images from a healthy volunteer, obtained with successive echoes, cardiac-gated spin echo, delay of 200 msec, section thickness of 5 mm, and FOV of 25 cm. Phase- (horizontal) and frequency- (vertical) encoding directions contain 128 × 512 steps. **(a)** TE of 30 msec (first echo). CSF appears darker than the spinal cord. A dark band is visible centrally in the cord and corresponds to a valley in the histogram. Pixel size is approximately one-fourth the spinal cord diameter. **(b)** TE of 60 msec (second echo). Even-echo rephasing of flowing CSF, which is almost isointense with the spinal cord. The mid-cervical spinal canal is six times the pixel size and contains two dark parallel bands. **(c)** Same sequence as **b**. Upper cervical canal is eight times the pixel size and contains three bands.

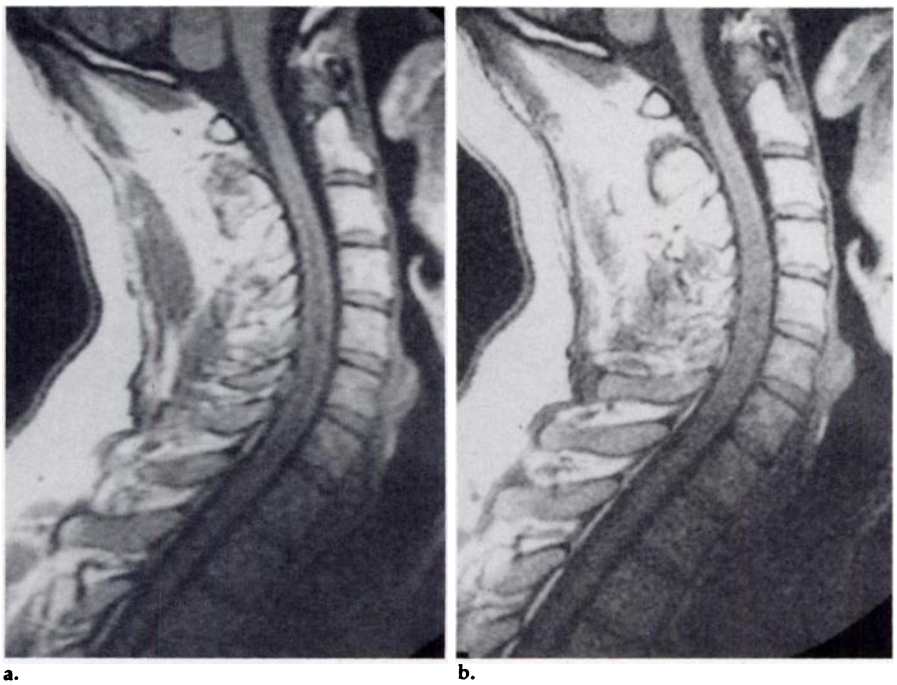

a. b.

**Figure 3.** Sagittal images of cervical spine in a 44-year-old man with fusiform cord enlargement. Ungated spin echo, section thickness of 5 mm, FOV of 25 mm, and SE 250/26 were used. **(a)** Phase- (horizontal) and frequency- (vertical) encoding directions contain 128 × 512 steps. A prominent dark band is seen centrally within the spinal cord. Sagittal spinal cord diameters are approximately four and five times the pixel size at the upper and lower cervical regions, respectively. **(b)** Sampling increased to 256 × 512. The dark central band is no longer seen.

and fat due to differences in their Larmor frequencies. This artifact appears as misregistration along the frequency axis and has no associated ripples. Artifacts due to motion appear as ghost images with variable periodicity along the phase axis only.

The present data indicate that sampling can lead to several different patterns of the Gibbs phenomenon in MR imaging of the spine. These patterns are affected by various factors such as object-to-pixel ratio, edge contrast, edge sharpness, and type of data filtering. The object-to-pixel size ratio is determined with the spatial sampling frequency. Edge contrast is affected by pulsing sequence parameters (TE, TR), relative tissue characteristics across the edge (relaxation times T1, T2), and physiologic factors, such as flow. Edge sharpness depends on the geometry of the structure visualized, section thickness, and section offset. Filtering the image data can decrease the ripples, but not without the loss of spatial resolution (2, 6).

A single midline central band of decreased intensity was observed along the length of the spinal cord when the pixel width was approximately one-fourth the spinal cord diameter. In this case, the wavelength of the oscillations produced a peak near each edge of the spinal cord and a central depression (Fig. 6). A similar effect was noted in the phantom image (Fig. 5). The resultant change in signal intensity across the spinal cord can thus approach up to 18% of the edge contrast. Reducing the pixel size by increasing the number of samples in the horizontal direction may lead to more complex patterns, such as two or more parallel bands along the length of the spinal cord. In general, when the object-to-pixel size ratio is equal to $N$, there should be $[(N/2)-1]$ artifactual bands (10, 15). On a T2-weighted image, the ripples may produce a factitiously thin spinal cord (Fig. 7). When $N$ is an even number, such as four or six, there are one or two central depressions within the object, respectively. However, when the magnitude of $N$ lies between two consecutive even numbers, the resulting ripple pattern can be more complex. The oscillations at the edges may not be significantly affected, but the central peaks or valleys can be altered or "stretched." The net effect depends on the degree to which the oscillations from opposite edges reinforce or cancel each other, which in turn depends on $N$. Spinal cord enlargement with an $N$ of five is possibly responsible for the dark central band prominence (Fig. 3a).

As the object-to-pixel size ratio approaches two, the secondary ripples disappear and only a central peak re-

mains (Fig. 6). Thus, the lack of edge overshoot and central bands does not necessarily imply that the Gibbs phenomenon is absent. If $N$ is reduced further, the effect of the resolving power also becomes important (9, 10). The result will be a loss in signal intensity from the object, which produces an incomplete peak or valley. This pattern is apt to occur when imaging relatively small structures (spinal subarachnoid space) or when large FOVs are used and may lead to false-negative or false-positive diagnostic results.

If the edge contrasts differ bilaterally, the magnitudes of the overshoots on opposite sides of the spinal cord may be unequal (Fig. 8). This is a direct result of the properties of the Gibbs phenomenon, in which the overshoot amounts to 9% of the signal-transition size (14–16). In spinal imaging, this may occur due to differences in CSF flow, partial volume averaging, presence of adjacent vascular structures, or pathologic conditions. Asymmetric signal intensities at the spinal cord edges may simulate demyelinating disease, tumor, or inflammatory processes. They may also mask the presence of true pathologic conditions, such as multiple sclerosis plaques.

Although bands of low or high signal intensity superimposed on the spine and spinal cord have been reported and thought to be CSF pulsation ghosting artifacts (17), they could be truncation effects. CSF motion spatially mismaps CSF signal intensity over the spine and spinal cord: The pattern depends on the relationship between heart rate and repetition time and on CSF pulsation amplitude. Unlike truncation artifacts, these bands propagate in the phase-encoding direction only, have no direct dependence on sampling, and are minimized with cardiac gating and rephasing (17). We have, however, observed bands on cardiac-gated images at all phases of the cardiac cycle, as well as on gated even-echo images and on ungated images acquired with MAST. Phantom studies also demonstrated bands with and without flow. The band patterns that we observed were directly dependent on sampling. In addition, switching phase and frequency directions caused a switch in the orientation of the bands overlying the vertebral bodies in all cases, which is compatible with a truncation effect.

When artifacts appear as a single midline band along the spinal cord, they can potentially be confused with a dilated central canal, central gray matter, syrinx, arteriovenous malformation, or longitudinal necrosis. Differentiation of artifacts from these other causes cannot always be done unless further imaging with different sampling rates is performed. A number of different imaging strategies may be used. Increasing the number of phase-encoding steps in the horizontal direction improves horizontal resolution but may increase imaging time (9). Interchanging the phase-encoding direction (usually the undersampled direction) with the frequency direction can increase the horizontal resolution without affecting the acquisition time, although motion artifacts and image wraparound may affect the regions of interest. Filtering the data may remove the high-frequency ringing but will lead to decreased


**Figure 4.** Sagittal images of cervical spine in a healthy volunteer obtained with different phase- and frequency-encoding directions, cardiac-gated spin echo, 1,000/30, and delay of 180 msec. Phase- and frequency-encoding directions contain 128 × 512 steps. Bright horizontal band crossing the cord at lower C-4 level is probably due to a swallowing artifact. **(a)** Phase- (horizontal) and frequency- (vertical) encoding directions contain 128 × 512 steps. Vertical dark bands are seen within the spinal cord and over the vertebral bodies. **(b)** Frequency- (horizontal) and phase- (vertical) encoding directions contain 512 × 128 steps. The dark central band within the spinal cord is no longer seen, and the vertical bands over the vertebral bodies are now horizontal.

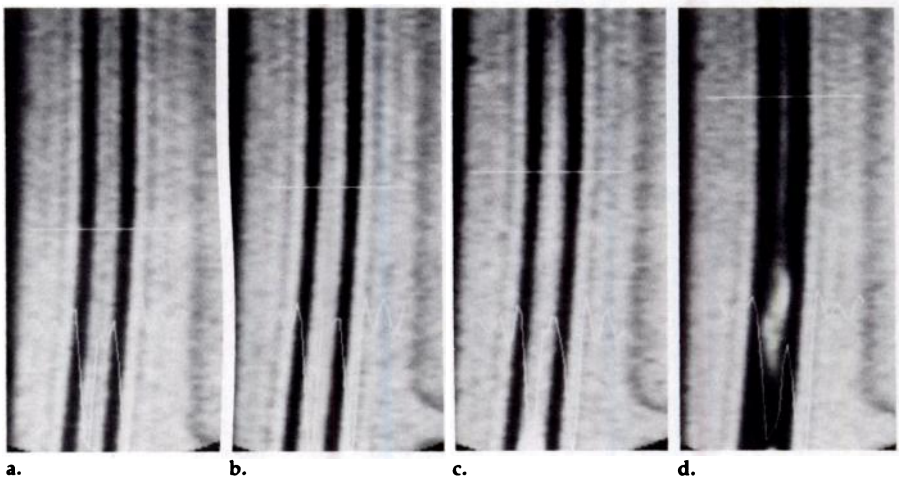


**Figure 5.** Images of flow phantom obtained at different flow velocities, with SE 700/26, phase- and frequency-encoding directions contain 128 × 512 steps and a FOV of 25 cm. Inner diameter of tube is 8 mm. **(a)** Stationary fluid. Dark parallel bands are seen that are parallel to the edges of the tube. A single dark central band is also seen within the tube. **(b)** Flow velocity of 0.5 cm/sec. Image shows no definite change. **(c)** Velocity of 2.0 cm/sec. Signal changes within the tube are noted, but the bands parallel to the edges of the tube remain unchanged. **(d)** Velocity of 6.0 cm/sec. Increasing areas of signal void within the lumen are now present, especially peripherally. The bands parallel to the tube appear unchanged. No new bands are seen.

spatial resolution by smoothing the image (2, 6). Anatomic and physiologic considerations may also augment diagnostic accuracy. Syringes or cavities may have associated findings such as spinal cord enlargement, intracavitary septations, Arnold-Chiari malformation, or spinal cord tumor or nodule (18). Arteriovenous malformations tend to be tortuous and may not be in the midline of the spinal cord. If an appropriate imaging sequence is used, arteriovenous malformations and syringes may show evidence of flow (19, 20). Longitudinal necrosis is usually accompanied by disk disease or spinal cord compression (21, 22).

The accuracy of both spatial and intensity measurements involving anatomic structures, such as the spinal cord and spinal canal, can be affected by the Gibbs phenomenon. Gray-level variations in MR images may also interact with the Gibbs phenomenon and affect the visual determination of anatomic boundaries. Additional sources of error include radio-frequency and field inhomogeneity (23). Although for the continuous Fourier transform the position of the first peak relative to the edge is affected by sampling (Fig. 6), the inflexion points of the reconstructed curves are not (14, 15). Edge determination with inflexion points could thus augment the accuracy of object-size measurements if aliasing errors created by discrete sampling are minimized. Similarly, localized measurement of signal intensity within an object could be most accurately determined at the inflexion points of the ripples. ■

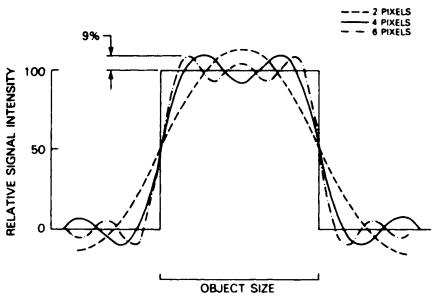


**Figure 6.** Effect of sampling on signal intensity pattern (as reconstructed with Fourier transform) shows changing number of pixels across object dimensions. With object-to-pixel size ratios of two, four, and six, there are zero, one, and two central depressions in the intensity profiles, respectively.

**Acknowledgments:** The authors express their great appreciation to Shirley Yang, M.D., for her very valuable help. Special thanks are extended to Dan Shook, M.S., for his assistance with the phantom studies. We are also grateful for the assistance of the MR technicians in the Department of Radiology at the National Institutes of Health, in particular, Brian Petrie, R.T., Graham Morrison, R.T., and Ron White, R.T.

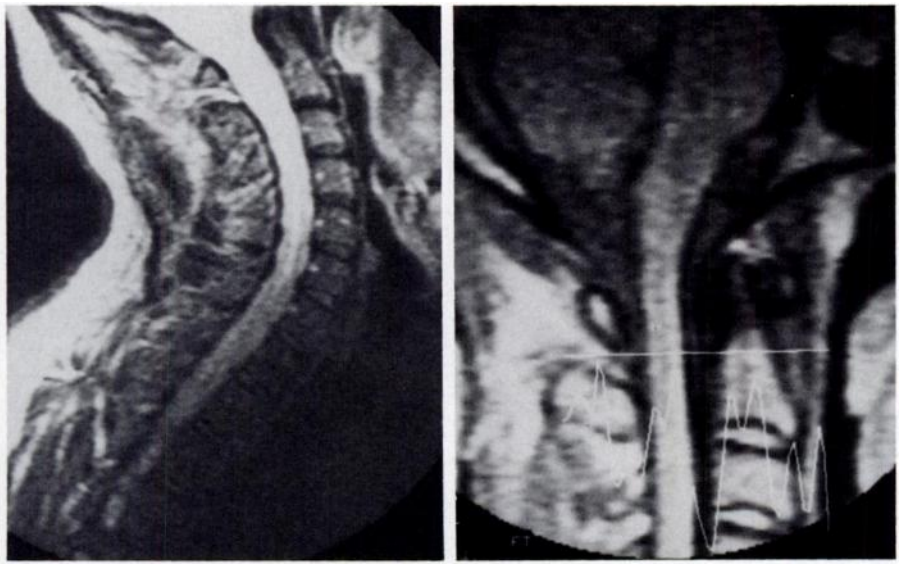

**7.** **8.**

**Figures 7, 8.** **(7)** Sagittal image of cervical spine (same patient as in Fig. 3) 10 days after surgery. Ungated SE with MAST, section thickness of 5 mm, FOV of 25 cm, phase- (horizontal) and frequency- (vertical) encoding directions contain 128 × 512 steps, and SE 2,000/100 were used. CSF is isointense with spinal cord. Two dark central bands are seen in the spinal canal the diameter of which is approximately six times the pixel size. Note the factitiously thin spinal cord (cord diameter appeared normal on corresponding T1-weighted image). **(8)** Effect of asymmetric intensity profiles in sagittal cervical spinal cord images from a healthy volunteer. Section thickness of 5 mm, FOV of 25 cm, phase- (horizontal) and frequency- (vertical) encoding directions contain 128 × 512 steps, gated SE 978/30, and a delay of 200 msec were used. Intensity profile shows that the magnitude of overshoot at the anterior edge of the spinal cord is larger than that at the posterior edge (asymmetric).

## References

1. Pusey E, Brown RKJ, Lufkin R, Solomon M, Hanafee W. Artifacts in magnetic resonance imaging: mechanisms and clinical significance (abstr.). Radiology 1985; 157(P):296.
2. Lufkin RB, Pusey E, Stark DD, Brown R, Leikind B, Hanafee WN. Boundary artifact due to truncation errors in magnetic resonance imaging. AJR 1986; 147:1283–1287.
3. Bellon EM, Haacke EM, Coleman PE, Sacco DC, Steiger DA, Gangarosa RE. Magnetic resonance artifacts: a review. AJR 1986; 147:1271–1281.
4. Hastrup W, Porter BA, Olson DO, et al. Classification and investigation of artifacts in magnetic resonance imaging (abstr.). Radiology 1985; 157(P):397.
5. Schultz CL, Alfidi RJ, Nelson AD, Kopiwoda SY, Clampitt ME. The effect of motion on two-dimensional Fourier transformation on magnetic resonance images. Radiology 1984; 152:117–122.
6. Wood ML, Henkelman RM. Truncation artifacts in magnetic resonance imaging. Magn Reson Med 1985; 2:517–526.
7. Kumar A, Welti D, Ernst J. NMR Fourier zeugmatography. J Magn Reson 1975; 18:69–83.
8. Flannigan BD, Rauschning W, Lufkin R, Wilson GH, Bradley WG. High resolution MR imaging and anatomy of the cervical spine (abstr.). Radiology 1985; 157(P):249.
9. Bradley WG, Kortman KE, Crues JV. Central nervous system high resolution magnetic resonance imaging: effect of increasing spatial resolution on resolving power. Radiology 1985; 156:93–98.
10. Schenck JF, Hart HR, Foster TH, Edelstein WA, Hussain MA. High resolution magnetic resonance imaging using surface coils. Magn Reson Annu 1986; 123–159.
11. Pattany PM, Phillips JJ, Chiu LC, et al. Motion artifact suppression technique (MAST) for MR imaging. J Comput Assist Tomogr 1987; 11:369–377.
12. Haacke EM, Lenz GW. Improving MR image quality in the presence of motion by using rephasing gradients. AJR 1987; 148:1251–1258.
13. Edelman RR, Wedeen VJ, Davis KR, et al. Multiphasic MR imaging: a new method for direct imaging of pulsatile CSF flow. Radiology 1986; 161:779–783.
14. Bracewell RN. The Fourier transformation and its applications. New York: McGraw-Hill, 1978; 211, 377.
15. Carslaw HS. An introduction to the theory of Fourier series and integrals. New York: Dover, 1930; 289–310.
16. Gibbs JW. Fourier's series. Nature 1898; 59(1522):200.
17. Rubin JB, Enzmann DR, Wright A. CSF-gated MR imaging of the spine: theory and clinical implementation. Radiology 1987; 163:784–792.
18. Di Chiro G, Doppman JL, Dwyer AJ, et al. Tumors and arteriovenous malformations of the spinal cord: assessment using magnetic resonance. Radiology 1985; 156:689–697.
19. Enzmann DR, Rubin JB, DeLaPaz R, Wright A. Cerebrospinal fluid pulsations: benefits and pitfalls in MR imaging. Radiology 1986; 161:773–778.
20. Kucharczyk W, Kelly WM, Davis DO, Norman D, Newton TH. Intracranial lesions: flow-related enhancement on MR images using time of flight effects. Radiology 1986; 161:767–772.
21. Hashizume Y, Iljima S, Kishimoto H, Hirano T. Pencil-shaped softening of the spinal cord: pathologic study in 12 autopsied cases. Acta Neuropathol 1983; 61:219–224.
22. Jinkins JR, Bashir R, Al-Mefty O, Al-Kawi MZ, Fox JL. Cystic necrosis of the spinal cord in compressive cervical myelopathy: demonstration by iopamidol CT-myelography. AJNR 1986; 7:693–701.
23. Zhu XP, Checkley DR, Hickey DS, Isherwood I. Accuracy of area measurements made from MR images compared with CT. J Comput Assist Tomogr 1986; 10(1):96–102.